ECCOMAS Congress 2016
VII European Congress on Computational Methods in Applied Sciences and Engineering
M. Papadrakakis, V. Papadopoulos, G. Stefanou, V. Plevris (eds.)
Crete Island, Greece, 5–10 June 2016

MODELLING OF UNSTEADY SECONDARY VORTICES GENERATED BEHIND THE RADIAL GAP OF THE AXIAL TURBINE BLADE WHEEL

Straka P.[1]

[1]Aerospace Research and Test Establishment, Plc.
Beranových 130, 19905 Prague, Czech Republic
e-mail: straka@vzlu.cz

Keywords: EARSM, hybrid RANS/LES, axial turbine stage, secondary flows.

Abstract. *The paper deals with application of the linear eddy viscosity model, the nonlinear explicit algebraic Reynolds stress model and the hybrid RANS/LES model for computation of flow in an axial turbine stage with radial gaps under the stator and above the rotor blade. Results show that the nonlinear explicit algebraic Reynolds stress model allows to describe deformation of the secondary vortices and their breakdown into smaller structures while the linear eddy viscosity model doesn't have this capability. Only hybrid RANS/LES model describes decay of the secondary vortices which interact with the rotor blade. This capability is necessary for good prediction of distribution of the turbine stage efficiency behind the rotor blade.*

1 INTRODUCTION

The axial steam turbine of low power (around hundreds kilowatts to units megawatts) are typically designed in configuration with the drum-type rotor. It means that the rotor blades are carried directly by the rotor of large diameter as it is depicted in figure 1. In case of low power turbines, in order to reduce a production costs a blades with free ends that are not equipped with the shroud are still in use. For more reduction of the production cost the prismatic blades are sometimes used as it is in the present work. In this configuration it is necessary to maintain the radial gap under the hub-end of the stator blades and above the tip-end of the rotor blades.

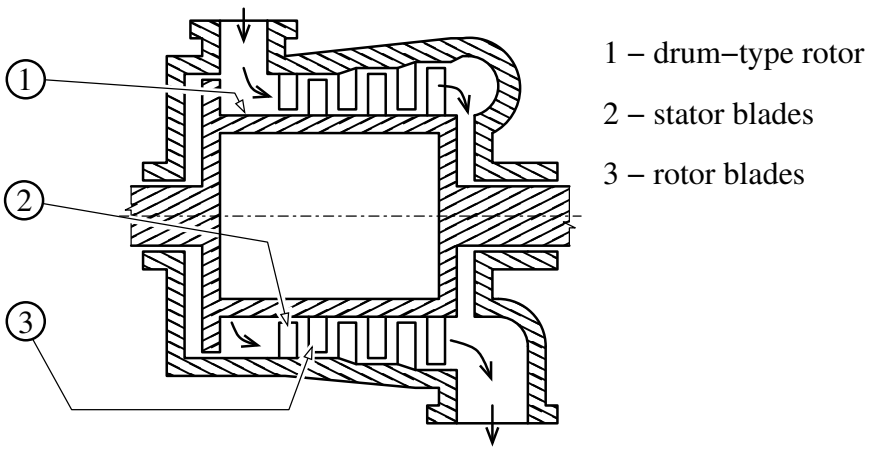

Figure 1: Scheme of the low power axial steam turbine with the drum-type rotor.

Flow through the radial gap generates an intensive secondary vortices which interacts with following blade wheel. This interaction leads to strong swirl of flow field in the peripheral parts of the blade span and it has major impact on the efficiency of the turbine stage. In [1] there was shown that drop in the efficiency due to interaction of the rotor blades with the secondary flows is up to ten percent. Prediction of the interaction of blade with the secondary flows strongly depends on used turbulence model. In industrial applications, such as this, it is usual to solve system of RANS (Reynolds Averaged NavierStokes) equations, which is closed by two-equation turbulence model (such as $k-\omega$). In [2] there was studied mechanism of the interaction between the rotor blades and the secondary vortices generated behind the radial gap under the stator blade using the $k-\omega$ model of Kok (2000) [3]. This model is based on linear relation for the Reynolds stress tensor. Although this model has provided interesting results, comparison with the experimental data revealed some differences in span-wise distribution of the efficiency behind the rotor blade. Therefore in [4] there was compared prediction of the secondary vortices development using the linear turbulence model of Kok (2000) [3] and the nonlinear EARSM (Explicit Algebraic Reynolds Stress Model) model of Rumsey & Gatski (2001) [5]. It was found that the nonlinear EARSM model predicts deformation and unsteady behaviour of the secondary vortices, while the linear model doesn't have this capability. However, for better prediction of the interaction between the rotor blade and the secondary vortices generated behind the radial gap under the stator blade it is necessary to model not only deformation of large vortices but also their decay. Therefore in this work a hybrid RANS/LES model is used for modeling of the rotor blade/secondary vortices interaction beside the LEVM (Linear Eddie Viscosity Model) model of Kok (2000) and the nonlinear EARSM model of Rumsey and Gatski (2001).

2 GEOMETRIC SETUP

Figure 2 shows the computational domain with marked inlet and outlet boundaries and sliding mesh interface between stator and rotor parts of the computational domain. It is seen that the computational domain contains only one stator and one rotor blade. Such a reduction of the actual number of blades is achieved by method of scaling. The scale factor of the stator blade is given by $2N_s/(N_s + N_r)$, where N_s is real number of the stator blades and N_r is real number of the rotor blades. The scale factor of the rotor blade is defined analogously. In our case the scale factor is $0.9\overline{09}$ for the stator blade and $1.\overline{09}$ for the rotor blade. Note that scaling has no effect on static aerodynamics loading of the blades, because the pitch to chord ratio of blades is preserved. Scaling of the blade profile causes little change of the chord based Reynolds number, but it is minor problem in case of values of scale factors near 1. The method of scaling has, however, major impact on prediction of dynamic aerodynamic loading of the blades. Therefore this method is unusable in cases where such that prediction is a main scope. In our case we want to compare prediction of the rotor blade interaction with secondary vortices generated behind the radial gap under the hub-end of the stator blade using turbulence models with different closure formulas. So the scaling method is applicable here. After scaling, the chord of the stator blade is 29.0 mm and the chord of the rotor blade is 28.1 mm. The hub diameter is 330 mm and diameter of the outer casing is 430 mm. Between the hub-end of the stator blade and the hub-wal there is the radial gap of 1.4 mm. Also between the tip-end of the rotor blade and the outer casing there is the radial gap of 1.4 mm. The axial distance between the stator trailing edge and the rotor leading edge is 8 mm. The inlet boundary is placed 22 mm in front the stator leading edge and the outlet boundary is placed 22 mm behind the rotor trailing edge. The sliding mesh interface between stator and rotor parts of the computational domain is placed in the middle of the axial gap between the stator and the rotor blades.

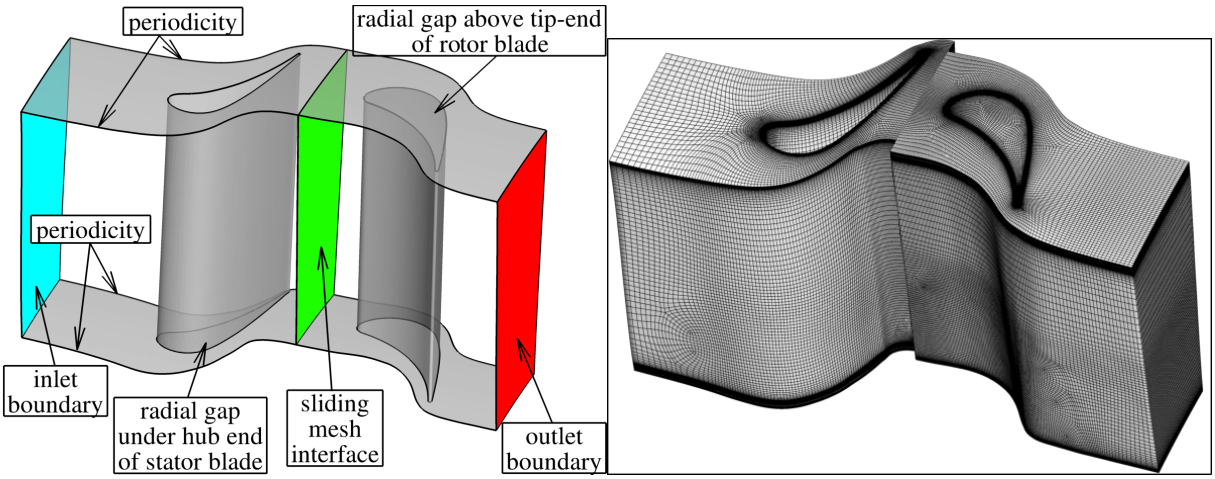

Figure 2: Scheme of the computational domain (left); computational mesh (right).

3 FLOW CONDITIONS

Presented results were calculated for the total/static expansion ratio 1.4, the velocity ratio $u/c_{is} = 0.6$ (u is the circumferential velocity at middle diameter and c_{is} is the isentropic velocity at the hub diameter behind the rotor trailing edge). It corresponds with the inlet total pressure 120 kPa, the outlet pressure 85.7 kPa, speed of revolutions 7430 RPM, the total inlet temperature

of 303 K. The isentropic outlet Mach number is $M_{is} = 0.7$, while the outlet isentropic Reynolds number based on blade chord is $Re_{is} \approx 3 \times 10^5$.

4 NUMERICAL APARATUS

Flow through the axial turbine stage is modeled as unsteady, 3D, compressible, viscous, fully turbulent flow of the perfect gas. Simulation is performed using the in-house numerical code based on solution of system of the RANS equation and two-equation $k - \omega$ turbulence model. Used numerical code [6, 7] is focused on turbomachinery application. The interface between stator and rotor part of the computational domain is performed via the "sliding mesh" method, where communication between stationary stator domain and rotating rotor domain is based on interpolation.

System of the governing equations reads:

$$\frac{\partial \rho}{\partial t} + \frac{\partial}{\partial x_j}\left(\rho u_j\right) = 0\,, \tag{1}$$

$$\frac{\partial}{\partial t}\left(\rho u_i\right) + \frac{\partial}{\partial x_j}\left(\rho u_j u_i + p\delta_{ij}\right) - \frac{\partial \tau_{ij}}{\partial x_j} = 0\,, \tag{2}$$

$$\frac{\partial e}{\partial t} + \frac{\partial}{\partial x_j}\left(\rho u_j(e+p) - u_k\tau_{kj} + q_j - d_j^t\right) = 0\,, \tag{3}$$

$$\frac{\partial}{\partial t}\left(\rho k\right) + \frac{\partial}{\partial x_j}\left(\rho u_j k - d_j^t\right) = P_k - D_k\,, \tag{4}$$

$$\frac{\partial}{\partial t}\left(\rho \omega\right) + \frac{\partial}{\partial x_j}\left(\rho u_j \omega - o_j^t\right) = P_\omega - \beta\rho\omega^2 + C_D, \tag{5}$$

where

$$p = (\kappa - 1)\left[e - \frac{\rho}{2}\left(u_1^2 + u_2^2 + u_3^2\right) - \rho k\right]\,,\; q_j = -\left(\frac{\mu}{\mathrm{Pr}} + \frac{\mu_t}{\mathrm{Pr_t}}\right)\frac{\kappa r}{\kappa - 1}\frac{\partial T}{\partial x_j}\,, \tag{6}$$

$$\tau_{ij} = \tau_{ij}^{lam} + \tau_{ij}^t\,,\; \tau_{ij}^{lam} = 2\mu\left(S_{ij} - \frac{1}{3}\frac{\partial u_k}{\partial x_k}\delta_{ij}\right)\,, \tag{7}$$

$$d_j^t = \left(\mu + \sigma_k \mu_t^{evm}\right)\frac{\partial k}{\partial x_j}\,,\; o_j^t = \left(\mu + \sigma_\omega \mu_t^{evm}\right)\frac{\partial \omega}{\partial x_j}\,, \tag{8}$$

$$P_k = \min\left(2\mu_t S^2,\, 2\mu_t \Omega^2,\, 20 D_k\right)\,,\; P_\omega = \gamma\frac{\omega}{k}P_k\,,\; C_D = \sigma_d\frac{\rho}{\omega}\max\left(\frac{\partial k}{\partial x_j}\frac{\partial \omega}{\partial x_j},\, 0\right)\,, \tag{9}$$

$$\mu = 1.72 \times 10^{-5}\left(\frac{T}{273.15}\right)^{0.754}\,, \tag{10}$$

$$\mu_t^{evm} = \rho\frac{k}{\omega}\,, \tag{11}$$

$$S = \sqrt{2S_{ij}S_{ij}}\,,\; \Omega = \sqrt{2\Omega_{ij}\Omega_{ij}}\,,\; S_{ij} = \frac{1}{2}\left(\frac{\partial u_i}{\partial x_j} + \frac{\partial u_j}{\partial x_i}\right)\,,\; \Omega_{ij} = \frac{1}{2}\left(\frac{\partial u_i}{\partial x_j} - \frac{\partial u_j}{\partial x_i}\right)\,. \tag{12}$$

The turbulent viscosity μ_t, the Reynolds stress tensor τ_{ij}^t and the destruction term D_k will be described later in caption 5.

System of equations (1) to (5) we can formally rewrite in vector form as follows:

$$\frac{\partial \mathbf{W}}{\partial t} + \frac{\partial \mathbf{F}_j}{\partial x_j} = \mathbf{Q}\,, \tag{13}$$

where $\mathbf{W}$ is vector of the conservative variables, $\mathbf{F}$ is vector of the inviscid and viscous fluxes and $\mathbf{Q}$ is vector of the source terms. System (13) is discretized using the cell-centered finite-volume method on multi-block structured mesh of hexahedral cells. Temporal discretization is

performed using the second-orded backward Euler formula in implicit form, which is realized through a dual iterative process:

$$\left(\frac{3}{2}\mathbf{I} + \Delta t \, \frac{\partial \mathbf{R}_i^{n,\nu}}{\partial \mathbf{W}_i^{n,\nu}}\right) \Delta \mathbf{W}_i^{n,\nu+1/2} + \Delta t \sum_{j=1}^{6} \frac{\partial \mathbf{R}_i^{n,\nu}}{\partial \mathbf{W}_j^{n,\nu}} \Delta \mathbf{W}_j^{n,\nu+1/2} =$$

$$= -\frac{3\mathbf{W}_i^{n,\nu} - 4\mathbf{W}_i^{n} + \mathbf{W}_i^{n-1}}{2} - \Delta t \, \mathbf{R}_i^{n,\nu} \,, \tag{14}$$

where $\mathbf{W}^{n,0} := \mathbf{W}^n$, $\Delta \mathbf{W}^{n,\nu+1/2} = \Delta \mathbf{W}^{n,\nu+1} - \Delta \mathbf{W}^{n,\nu}$ and $\mathbf{W}^{n+1} := \mathbf{W}^{n,\nu^*}$, where $\mathbf{W}^{n,\nu^*}$ is a steady solution in the dual iterative process. In scheme (14) there n means the time level, Δt is the time step, ν is index of the dual iteration, i is index of current cell in the computational mesh, j is index of the neighbouring cells and $\mathbf{R}$ is the numerical approximation of the inviscid and the viscous fluxes:

$$\mathbf{R}_i = \frac{1}{V_i} \sum_{j=1}^{6} [\Phi^{inv}(\mathbf{W}_j^L,\ \mathbf{W}_j^R,\ \mathbf{n}_j) - \Phi^{vis}(\mathbf{W}_j^C,\ (\nabla \mathbf{W})_{D_j^{dual}},\ \mathbf{n}_j)] \, s_j \,. \tag{15}$$

The inviscid numerical fluxes Φ^{inv} are calculated using the exact solution of the 1D Rieman problem in normal direction to the cell edges. The viscous numerical fluxes Φ^{vis} are calculated using the central scheme and the gradient of the state vector $\nabla \mathbf{W}$ is calculated using the Green-Gauss theorem on a dual cells. Higher order of accuracy in space is obtained using linear reconstruction with the Van Leer's slope limiter.

The computational domain was discretized by structured multiblock mesh of 4.5 millions hexahedral cells which is displayed in figure 2.

5 CLOSURE FORMULA

As it was mentioned above, this work is focused on comparison of prediction of the blade/secondary flow interaction calculated using LEVM model of Kok (2000) [3], EARSM model of Rumsey and Gatski (2001) [5] and the hybrid RANS/LES method. The hybrid RANS/LES method according to Davidson and Peng (2003) [8] and Kok et al. (2004) [9] is used in this work. This approach uses one transport equation for the kinetic energy which plays role of the turbulent kinetic energy in RANS mode and the subgrid scale kinetic energy in LES mode. This kind of the hybrid RANS/LES methods is also called XLES (from eXtra Large Eddy Simulation).

5.1 LEVM model

This model is based on the Boussinesq approximation. The Reynolds stress tensor τ_{ij}^t is modeled as a linear function of the strain rate tensor S_{ij}:

$$\tau_{ij}^t = 2\mu_t \left(S_{ij} - \frac{1}{3}\frac{\partial u_k}{\partial x_k}\delta_{ij}\right) - \frac{2}{3}\rho k \delta_{ij} \,, \tag{16}$$

where the turbulent viscosity $\mu_t = \mu_t^{evm}$ is given by eq. (11). The destruction term D_k in eq. (4) and (9) is given as

$$D_k = \beta^* \rho k \omega \,. \tag{17}$$

The model constants: $\beta^* = 0.09$, $\beta = 0.075$, $\gamma = 0.5532$, $\sigma_k = 0.5$, $\sigma_\omega = 0.5$ and $\sigma_d = 0.5$ corresponds with the TNT $k - \omega$ turbulence model proposed by Kok (2000) [3].

5.2 EARSM model

In this model according to Rumsey and Gatski (2001) [5] the Reynolds stress tensor τ_{ij}^t is modeled as a quadratic function of the strain rate tensor S_{ij}:

$$\begin{aligned}\tau_{ij}^t = 2\mu_t\left(S_{ij} - \frac{1}{3}\frac{\partial u_k}{\partial x_k}\delta_{ij}\right) - \frac{2}{3}\rho k\delta_{ij} + 2\mu_t\Big[a_2a_4\left(S_{ik}\Omega_{kj} - \Omega_{ik}S_{kj}\right) \\ - 2a_3a_4\left(S_{ik}S_{kj} - \tfrac{1}{3}S_{kl}S_{lk}\delta_{ij}\right)\Big]\,.\end{aligned} \tag{18}$$

It is clear that eq. (18) extends relation (16) about anisotropy part (term in square brackets). The turbulent viscosity μ_t is now given as

$$\mu_t = C_\mu\rho k\tau\,, \tag{19}$$

where the turbulent time scale τ is defined as

$$\tau = \max\left(\frac{1}{\beta^*\omega},\, C_\tau\sqrt{\frac{\mu}{\beta^*\rho k\omega}}\right)\,, \tag{20}$$

where $C_\tau = 6.0$ is a model constant. The nominal level of the variable coefficient C_μ in a zero-pressure-gradient log-layer is approximately 0.09. In general case value of C_μ is obtained by solving following cubic equation:

$$\left(-C_\mu\right)^3 + q_1\left(-C_\mu\right)^2 + q_2\left(-C_\mu\right) + q_3 = 0\,, \tag{21}$$

where

$$q_1 = -\frac{\gamma_1^*}{II_S\tau^2\gamma_0^*}\,,\; q_2 = \frac{1}{\left(2II_S\tau^2\gamma_0^*\right)^2}\left(\gamma_1^{*2} - 2II_S\tau^2\gamma_0^*a_1 - \tfrac{2}{3}II_S\tau^2a3_2 - 2II_\Omega\tau^2a_2^2\right), \tag{22}$$

$$q_3 = \frac{\gamma_1^*a_1}{\left(2II_S\tau^2\gamma_0^*\right)^2}\,,\; II_S = S_{kl}S_{lk}\,,\;\; II_\Omega = \Omega_{kl}\Omega_{lk}\,. \tag{23}$$

The correct root to choose from this equation is the root with the lowest real part. See [5] for more details. Other parameters are gived by:

$$a_1 = \tfrac{1}{2}\left(\tfrac{4}{3} - C_2\right)\,,\; a_2 = \tfrac{1}{2}\left(2 - C_4\right)\,,\; a_3 = \tfrac{1}{2}\left(2 - C_3\right)\,,\; a_4 = \tau/\left(\gamma_1^* + 2\gamma_0^*C_\mu S^2\tau^2\right), \tag{24}$$

$$\gamma_0^* = C_1^1/2\,,\;\; \gamma_1^* = \tfrac{1}{2}C_1^0 + \left(\tfrac{C_{\varepsilon2} - C_{\varepsilon1}}{C_{\varepsilon1} - 1}\right)\,, \tag{25}$$

where $C_{\varepsilon1} = 1.44$, $C_{\varepsilon2} = 1.83$, $C_1^0 = 3.4$, $C_1^1 = 1.8$, $C_2 = 0.36$, $C_3 = 1.25$ and $C_4 = 0.4$.

The destruction term D_k in eq. (4) and (9) is given by eq. (17).

The model constants are now: $\beta^* = 0.09$, $\beta = 0.0747$, $\gamma = 0.53$, $\sigma_k = 1$, $\sigma_\omega = 0.5339$ and $\sigma_d = 0.5$.

5.3 XLES model

The hybrid RANS/LES method according to Davidson and Peng (2003) [8] and Kok et al. (2004) [9] switches between the system of RANS equations closed by two-equation turbulence model of Kok (2000) [3] and LES when computational mesh is fine enough to simulation of large turbulent eddies. The sub-grid scale model of LES is based on transport equation for the sub-grid scale turbulent energy given by eq. (4), where the destruction term D_k is given as

$$D_k = \max\left(\beta^*\rho k\omega,\; \frac{\rho\sqrt{k^3}}{C_{DES}\Delta}\right)\,, \tag{26}$$

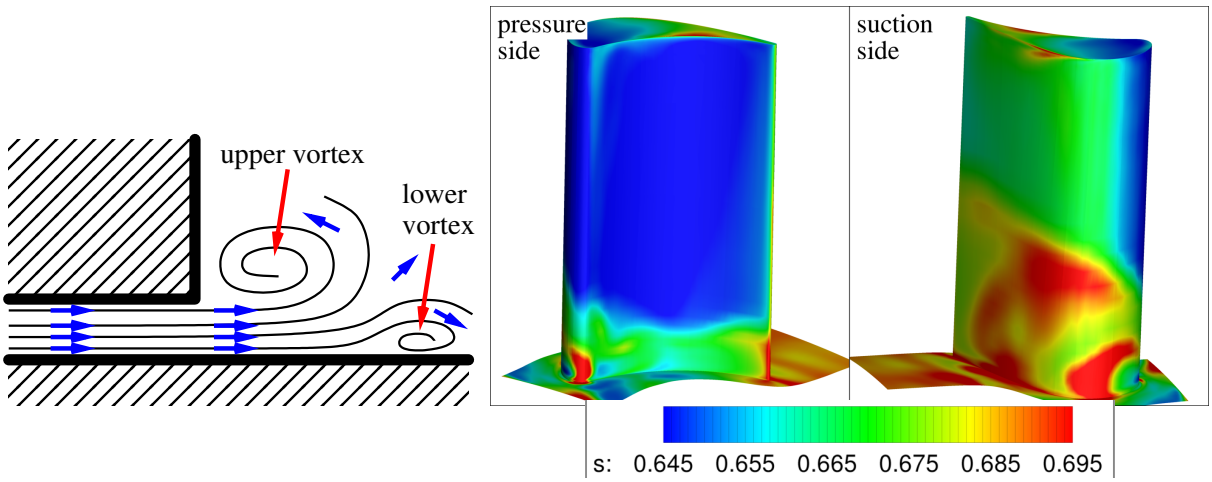

Figure 3: Scheme of flow behind the radial gap under the stator blade (left); distribution of the dimensionless entropy index $s = p/\rho^\kappa$ on the rotor blade surface (right).

where the local grid size Δ is defined by $\Delta = \max(\Delta_\xi, \Delta_\eta, \Delta_\zeta)$ where Δ_ξ, Δ_η and Δ_ζ are the distances between the cell faces in local ξ, η and ζ grid line directions. Constant $C_{DES} = 0.6086$ is chosen according to Kubacki et al. (2013) [10]. Note that in XLES approach k is either the turbulent energy in RANS mode or the sub-grid scale energy in LES mode.

The modeled stress tensor (Reynolds stress tensor in RANS mode, sub-grid scale stress tensor in LES mode) is given by eq. (16) where

$$\mu_t = \min\left(\rho k/\omega,\ \rho\beta^*\sqrt{k}C_{DES}\Delta_{LES}\right) \tag{27}$$

is either the turbulent viscosity in RANS mode or the sub-grid scale viscosity in LES mode. In eq. (27) there is $\Delta_{LES} = (\Delta_\xi\Delta_\eta\Delta_\zeta)^{1/3}$. It is evident that the solution is independent on equation (5) in LES mode although equation (5) is solved.

6 ADAPTATION OF NUMERICAL METHOD FOR XLES MODELLING

As it was mentioned above, the discretization scheme is based on the finite volume method in cell-centered form, where the inviscid numerical fluxes Φ^{inv} are calculated using the exact solution of the 1D Rieman problem in normal direction to the cell edges. Although numerical methods based on exact or approximate solution of the Riemann problem have good features for RANS modelling, they are too dissipative for using in LES approach. Therefore a central differencing is used in this work for suppression of the native numerical dissipation.

Let $\Phi^{inv}(\mathbf{W}^L_{i+1/2},\ \mathbf{W}^R_{i+1/2},\ \mathbf{n}_{i+1/2})$ is the inviscid numerical flux through cell face between i-th and (i+1)-th cells which is based on solution of the Riemann problem where $\mathbf{W}^L_{i+1/2}$ and $\mathbf{W}^R_{i+1/2}$ denotes state vectors extrapolated to the cell face from the left and right in means of linear reconstruction with the slope limiter. Let $\mathbf{W}^C_{i+1/2}$ is the state vector at the cell face computed as an average value of the state vectors in centers of i-th and (i+1)-th cells. The central differencing is obtained by replacing of $\mathbf{W}^L_{i+1/2}$ and $\mathbf{W}^R_{i+1/2}$ by $\mathbf{W}^{CL}_{i+1/2}$ and $\mathbf{W}^{CR}_{i+1/2}$ where $\mathbf{W}^{CL}_{i+1/2} = \psi\mathbf{W}^C_{i+1/2} + (1-\psi)\mathbf{W}^L_{i+1/2}$ and $\mathbf{W}^{CR}_{i+1/2} = \psi\mathbf{W}^C_{i+1/2} + (1-\psi)\mathbf{W}^R_{i+1/2}$. Parameter ψ is given as

$$\psi = \begin{cases} 0 & \text{for } L_t < L_{DES} \quad \text{(RANS mode)}, \\ [0.5 - 0.5\cos(2\pi(1 - L_{DES}/L_t))]^2 & \text{for } L_t \geq L_{DES} \quad \text{(LES mode)}, \end{cases} \tag{28}$$

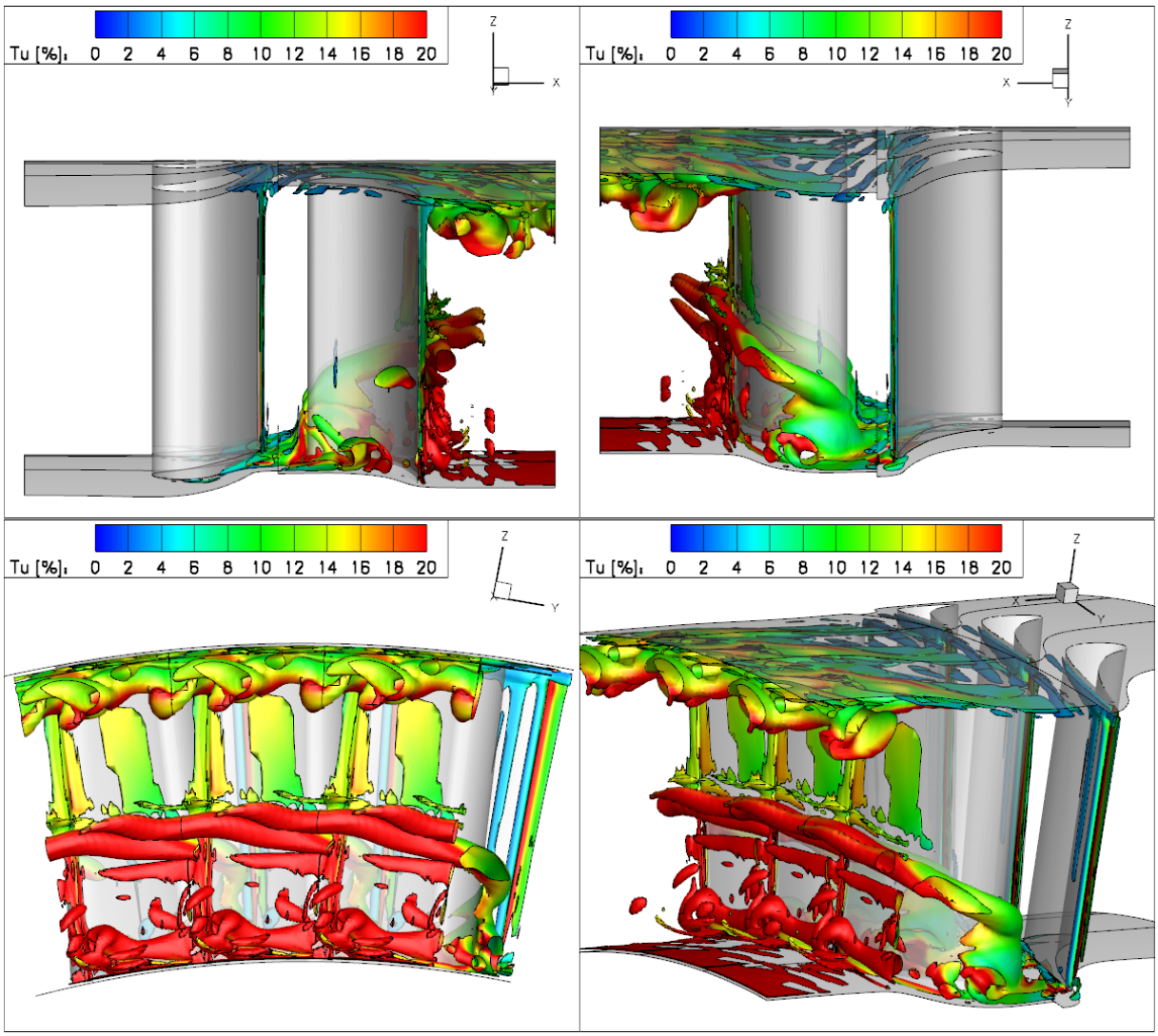

Figure 4: LEVM – instantaneous isosurfaces of $(|\Omega|^2 - |S|^2)$ colored by local turbulence intensity.

where $L_t = \sqrt{k}/\beta^*\omega$ is the turbulent length scale and $L_{DES} = C_{DES}\Delta_{DES}$ is the sub-grid length scale.

7 COMPUTATIONAL RESULTS

In figures 4 to 6 there are shown an instantaneous isosurfaces of $(|\Omega|^2 - |S|^2)$ colored by local turbulence intensity for LEVM, EARSM anf XLES models. The local turbulence intensity is related to the modeled part of the turbulent or sub-grid scale kinetic energy. In figures 4 to 6 there we can recognize two strong sources of secondary vortices. These are the radial gaps under the hub-end of the stator blade and above the tip-end of the rotor blade. We focus now on the radial gap under the stator blade. The effect of flow through the radial gap under the stator blade is such that stream flowing from the radial gap generates (in interaction with main stream in blade channel) massive vortex above the stream and beside the vertical surface of the suction side as illustrates a scheme in left part of figure 3. This upper vortex is in given regimes and geometrical configurations intensive enough to deform the stream flowing from the radial gap which leads to separation of the stream from the wall and to generation of the

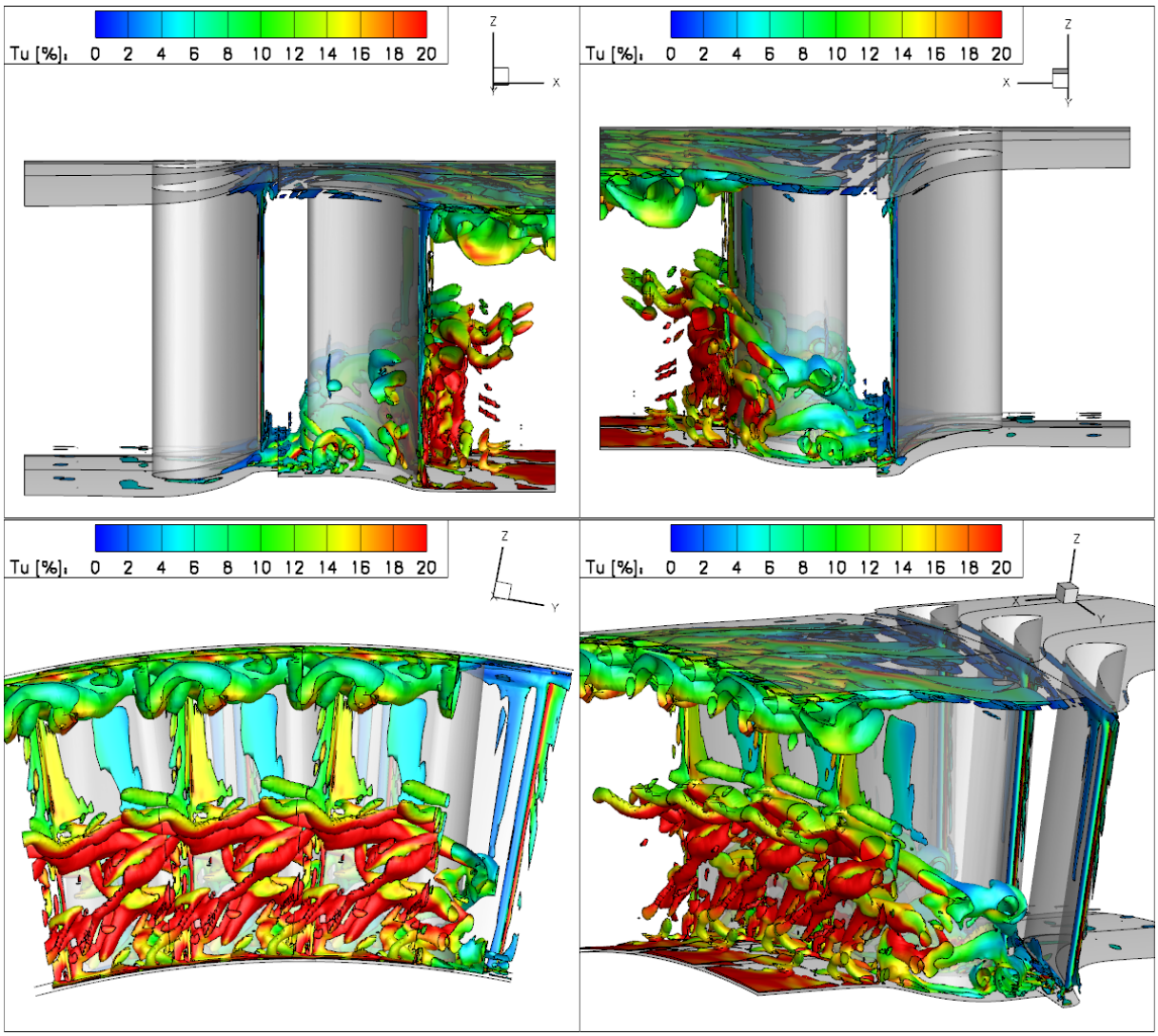

Figure 5: EARSM – instantaneous isosurfaces of $(|\Omega|^2 - |S|^2)$ colored by local turbulence intensity.

other vortex under the stream. Both vortices then interact with the rotor blade so that they deforms in upward direction and they are carried on the suction side almost up to half of the span. This causes increase of the dissipation rate on the lower half of span on the suction side, as illustrates distribution of the dimensionless entropy index $s = p/\rho^\kappa$ (computed from the normalized pressure and density) on the rotor blade surface that is shown in right part of figure 3. The LEVM model predicts the interaction of the rotor blade with the secondary vortices so that the secondary vortices remains more or less compact and undeformed. We can identify them in figure 4 behind the rotor blades at the middle of span. The EARSM model predicts deformation of the secondary vortices which interact with the rotor blades and their breakdown into smaller structures as is shown in figure5. In case of the XLES model we can observe a decay of the secondary vortices during the interaction with the rotor blade as is shown in figure 6. We can also see that in case of the XLES model the local turbulence intensity, that relates to the modeled kinetic energy, is smaller compared to the LEVM and the EARSM models. This is because a larger part of the kinetic energy is directly resolved as a nonstationary fluctuations. We can also recognize in figures 4 to 6 vortex structures behind the rotor blade at upper twenty

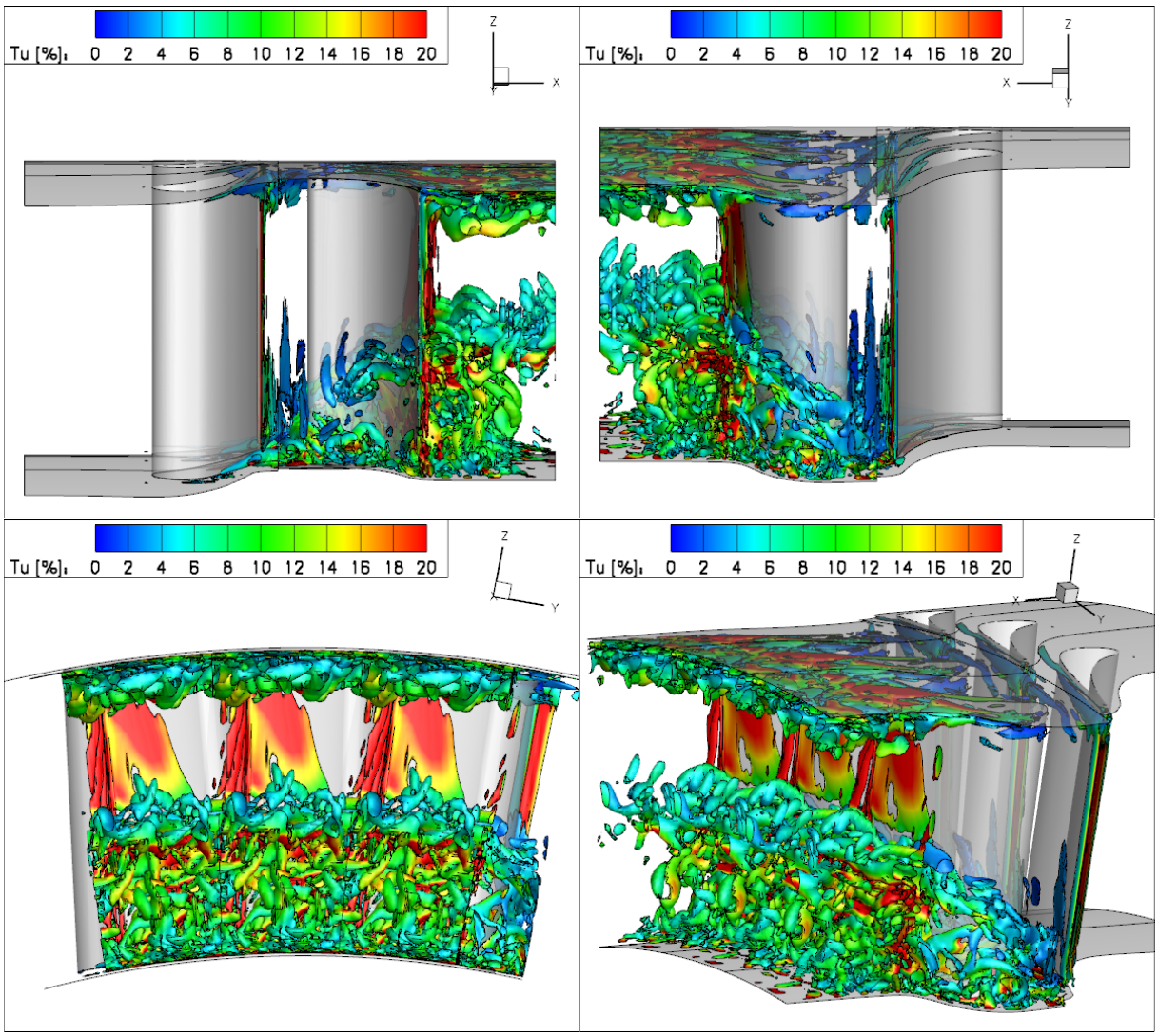

Figure 6: XLES – instantaneous isosurfaces of $(|\Omega|^2 - |S|^2)$ colored by local turbulence intensity.

percent of span, that arise behind the radial gap above the rotor blade.

In figure 7 there is shown an instantaneous and time averaged (in rotating frame) distribution of the total-total efficiency η_{TT} in an angular section 11 mm behind the trailing edge of the rotor blade. The total-total efficiency is defined as $\eta_{TT} = (T_{T0} - T_T)/(T_{T0} - T_{Tis})$ where T_{T0} is the inlet total temperature, T_T is local total temperature and T_{Tis} is the total isentropic temperature. On time averaged distribution there is a local maximum of the efficiency approximately at one quarter of the span in case of the LEVM and the EARSM models. This locale maximum is supressed in case of the XLES model due to decay of the secondary vortices into smaller and smaller structures which fill almost uniformly lower half of the span. This behaviour much better corresponds with the experimental data (from [1, 2]) than results of the LEVM and the EARSM models as shown in figure 8, where is shown a span-wise distribution of the circumferential averaged total-total efficiency. From figure 8 it is evident that all used models overpredict the efficiency about four percent between sixty and eighty percent of the span. It is an area which is not affected by secondary vortices. The overprediction of the efficiency may be due to insufficient resolving of the wakes.

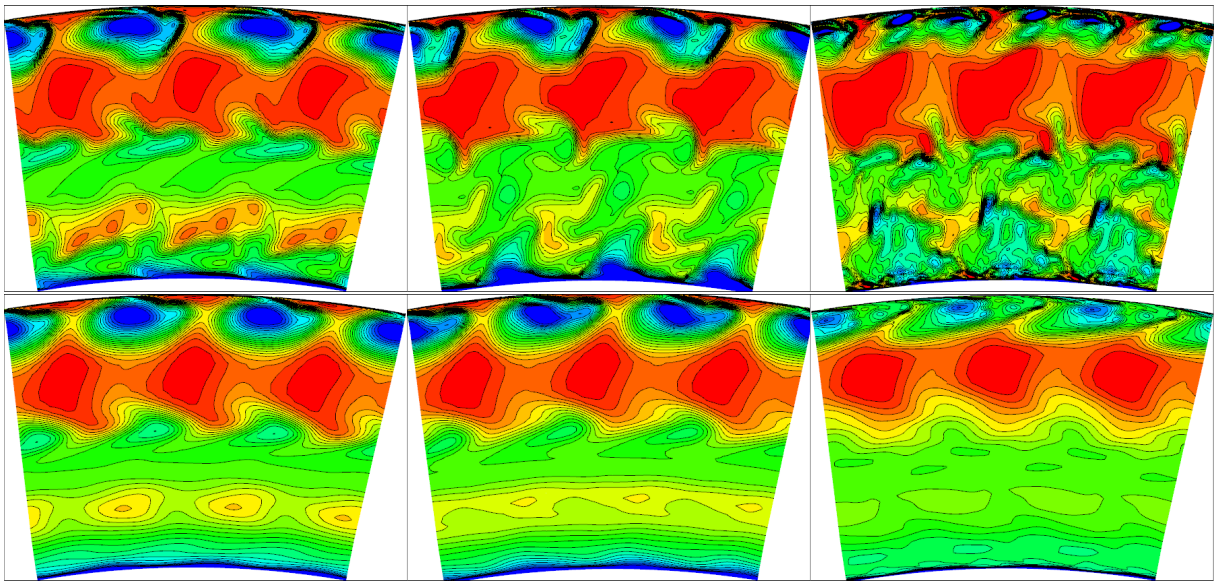

Figure 7: Distribution of the total-total efficiency in angular section 11 mm behind the trailing edge of the rotor blades. LEVM (left column); EARSM (middle column); XLES (right column); instantaneous distribution (top row); time averaged distribution – in rotating frame (bottom row).

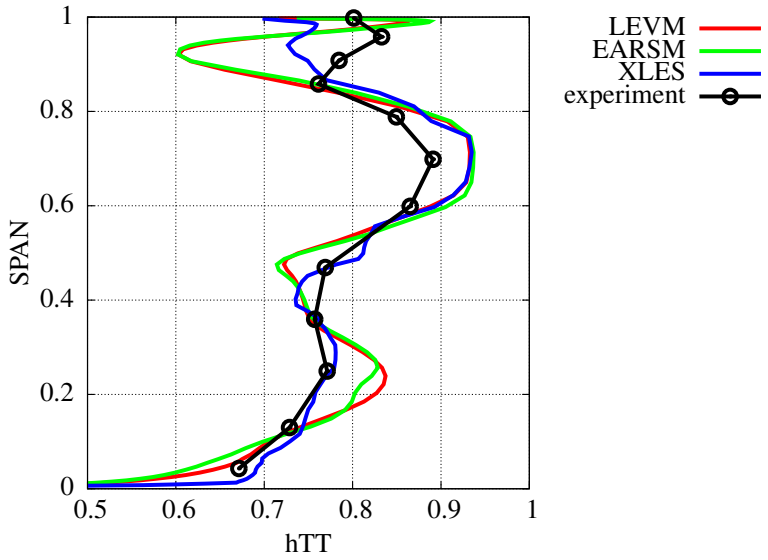

Figure 8: Span-wise distribution of the circumferentially averaged total-total efficiency in section 11 mm behind the trailing edge of the rotor blade – comparison with the experimental data.

8 CONCLUSIONS

Three kinds of turbulence models were applied for computation of flow in axial turbine stage with prismatic blades which are not equipped with the shroud. The LEVM model which is based on linear relation for the Reynolds stress tensor, the nonlinear EARSM model which uses a quadratic relation for the Reynolds stress tensor and the XLES model which combines RANS approach near the wall and LES approach for simulation of large vortices. Results shown that the LEVM model does not predict deformation and breakdown of the secondary vortices generated behind the radial gap under the stator blade which interact with the rotor blade. Deformation of this vortices and their breakdown into smaller structures predicts the nonlinear EARSM model. Better agreement with the experimental data is achieved using the XLES model which describes decay of the secondary vortices.

ACKNOWLEDGEMENT

This work was supported by the Long-term Framework Advancement Plan provided by the Ministry of Industry and Trade of the Czech Republic.

REFERENCES

[1] P. Straka, M. Němec, T. Jelínek, Investigation of flow in axial turbine stage without shroud-seal. *EPJ Web of Conferences,* , **92**, 02088, 2015.

[2] P. Straka, M. Němec, Influence of the radial gap under the stator blade on flow around the hub-end of the rotor blade. *Applied Mechanics and Materials*, **821**, 120–128, 2016.

[3] J. C. Kok, Resolving the dependence of freestream values for the k turbulence model. *AIAA Journal*, **38**, 7, 1292–1295, 2000.

[4] P. Straka, Numerical simulation of high-swirl flow in axial turbine stage. P. Dančová, M. Veselý eds. *Proc. Conf. Experimental Fluid Mechanics 2015*, 904–910, Prague, Czech Republic, 2015.

[5] C. L. Rumsey, T. B. Gatski, Recent turbulence model advances applied to multielement airfoil computations. *Journal of Aircraft*, **38**, 5, 904–910, 2001.

[6] P. Straka, Simulation of a 3D unsteady flow in an axial turbine stage. *EPJ web of Conferences*, **25**, 01090, 2012.

[7] P. Straka, Calculation of 3D unsteady flow in axial stage of low power experimental turbine. *Technical Report VZLU R-5904*, Prague, 2013, (in Czech).

[8] L. Davidson, S. H. Peng, Hybrid LES-RANS modelling: a one-equation SGS model combined with a $k-\omega$ model for predicting recirculating ows. *Int. Jour. Numer. Meth. Fluids*, **43**, 1003-1018, 2003.

[9] J. C. Kok, H. S. Dol, B. Oskam, H. van der Ven, Extra-large eddy simulation of massively separated flows. *AIAA paper*, 2004-264, 2004.

[10] S. Kubacki, J. Rokicki, E. Dick, J. Degroote, J. Vierendeels, Hybrid RANS/LES of plane jets impinging on a flat plate at small nozzle-plate distances. *Arch. Mech.*, **65**, 2, 143–166, 2013.